Research Article

ADVANCED PHOTONICS

# Spatiotemporal coherence engineering of light

**Xin Liu**,[a,b] **Weiran Li**,[a,b] **Sergey A. Ponomarenko**,[c,d,*] **Chunhao Liang**,[a,b] **Yaning Zhou**,[a,b] **Qiwen Zhan**,[e,f,*] **and Yangjian Cai**[a,b,*]

[a]Shandong Normal University, School of Physics and Optoelectronics, Shandong Provincial Key Laboratory of Light Field Manipulation Physics and Applications, Jinan, China
[b]Shandong Normal University, Collaborative Innovation Center of Light Manipulations and Applications, Jinan, China
[c]Dalhousie University, Department of Physics and Atmospheric Science, Halifax, Canada
[d]Dalhousie University, Department of Electrical and Computer Engineering, Halifax, Canada
[e]Westlake University, School of Engineering, Zhejiang Key Laboratory of 3D Micro/Nano Fabrication and Characterization, Department of Electronic and Information Engineering, Hangzhou, China
[f]University of Shanghai for Science and Technology, School of Optical-Electrical and Computer Engineering, Shanghai, China

**Abstract.** Structured light with sculpted spatial and temporal degrees of freedom (DoFs) provides unprecedented opportunities across diverse scientific disciplines and areas of technology. However, spatiotemporal shaping is currently limited to deterministic DoFs of coherent pulsed beams. In contrast, the spatiotemporal coherence manipulation of light sources has not made any comparable headway, leaving the potential of partially coherent space-time wave packets essentially unfulfilled to date. Herein, we demonstrate theoretically and experimentally that salient features of light sources, such as their coherence width and structure, can be precisely tailored in the space-time domain. We formulate a space-time analogue of the celebrated van Cittert–Zernike theorem and utilize it to realize partially coherent wave packets with nontrivially structured spatiotemporal coherence in the laboratory. The evolution of wave packets with structured spatiotemporal coherence in free space or dispersive media differs in fundamental ways from that of conventional quasimonochromatic light with reduced spatial coherence. Our work establishes a versatile framework for manipulating the coherence of light fields in space and time, thereby paving the way for experimental studies of dynamic and noninvasive imaging, robust information transmission, remote sensing, and nonlinear frequency conversion, all topical areas of growing importance in both fundamental optical physics and photonics applications.

Keywords: structured light; optical coherence; spatiotemporal light field; ultrafast optics; time-varying wave packets.

Received Mar. 18, 2026; revised manuscript received May 20, 2026; accepted for publication Jun. 12, 2026; published online Jul. 9, 2026.

© The Authors. Published by SPIE and CLP under a Creative Commons Attribution 4.0 International License. Distribution or reproduction of this work in whole or in part requires full attribution of the original publication, including its DOI.

[DOI: 10.1117/1.AP.8.4.046013]

## 1 Introduction

Coherence is an important fundamental concept in wave optics that quantifies the phase stability and correlation properties of light fields.[1] Unlike other deterministic DoFs of fully coherent light at the first order—such as intensity, wavefront, polarization, frequency, and angular momentum[2–4]—optical coherence measures the extent of statistical correlations of light fields at pairs of space-time points. The degree of optical coherence becomes particularly relevant to the description of partially coherent waves.[5] Recent advances in partially coherent beams have demonstrated a remarkable versatility of coherence engineering across a wide range of applications. Controlling spatial or temporal coherence of light has enabled robustness to signal degradation and enhanced depth perception in passive imaging systems,[6–14] strengthened data security and increased channel capacity in cryptography,[15–19] improved measurement stability and precision in optical metrology,[20–23] and boosted processing parallelism and scalability in optical computing,[24–26] among other emerging applications. Although coherence of light has been extensively explored using cutting-edge optical techniques, the manipulation of spatiotemporal coherence remains largely confined to spontaneous emission processes such as

*Address all correspondence to Sergey A. Ponomarenko, serpo@dal.ca; Qiwen Zhan, zhanqiwen@westlake.edu.cn; Yangjian Cai, yangjiancai@sdnu.edu.cn

stars, light-emitting diodes (LEDs), thermal emitters, photovoltaics, and luminescent materials.

With the rapid advancements in ultrafast optics, recent studies have begun to tap into the joint manipulation of spatial and temporal DoFs of light to control and characterize spatiotemporally structured optical wave packets.[27–29] Notable achievements there include the realization of space-time vortices carrying transverse orbital angular momentum,[30–32] propagation-invariant space-time light sheets with tunable group velocities,[33,34] veiled[35] and simultaneous spatial and temporal[36] Talbot revivals of spatiotemporal wave packets, toroidal light vortices exhibiting torus-shaped energy flow,[37–39] and optical combs with time-varying properties.[40,41] Collectively, these advances in manipulating the deterministic DoFs of light have, in turn, profoundly expanded the applicability of such DoFs to optical topology[42–45] and nonlinear processing.[46,47] At the same time, the authors of Ref. 48 demonstrated joint control of spatial and temporal coherence by applying spatiotemporal shaping techniques to broadband incoherent light. Specifically, space and time frequency correlations were imposed on the angular spectrum of an LED source to generate nondiffracting polychromatic space-time fields. Taking a more direct strategy, a recent advance in achieving spatiotemporal coherence with a white-light source has been realized by miniaturizing spiral phase plates and integrating them with structural color filters,[49] thereby enabling the generation of colored vortex beams. We stress, however, that the intrinsic incoherent structure of the source in Refs. 48, 49 remained unaltered. Hence, despite these advances, attaining complete control over the spatiotemporal coherence of structured optical wave packets presents a formidable challenge.

Here, we advance a paradigm for sculpting coherence properties of optical wave packets in space and time by formulating a spatiotemporal analogue of the celebrated van Cittert-Zernike theorem.[1] By leveraging complex incoherent modulation of an ultrashort chirped pulse, we generate statistically stationary wave packets with precisely tailored spatiotemporal coherence width and structure, including those associated with a Gaussian Schell-model and non-Gaussian correlated sources. Moreover, we show that the wave packets with engineered space-time coherence can exhibit unusual propagation behavior governed by the interplay of diffraction and medium dispersion. Our protocol unlocks a new dimension for spatiotemporal wave packet control associated with the space-time coherence DoF of light fields. The unveiled dimension may prove instrumental in exploring the evolution of stochastic pulses in complex time-varying media,[50,51] nonlinear synthesis,[52] and quantum coherence.[22,53,54]

## 2 Results

### 2.1 Spatiotemporal van Cittert-Zernike Theorem

We start by formulating a spatiotemporal analogue of the van Cittert-Zernike theorem. To this end, we consider an ensemble of random polychromatic light sheets propagating in a weakly dispersive linear medium. Within the paraxial and slowly varying envelope approximations, the electric field of any member of the ensemble can be expressed in terms of its envelope and pilot (carrier) wave as $U(x,t,z) = \Psi(x,t,z)e^{-i\omega_0 t + ik_0 z}$, where $\omega_0 = k_0 c = 2\pi c/\lambda_0$ denotes the carrier frequency. The envelope of the wave packet in any transverse plane $z = \text{const}$ within the medium can be represented by the integral (see Note 1 in the Supplementary Material),

$$\Psi(x,\tau,z) = (k_0/2\pi i z)^{1/2} \iint \Psi_0(x',\varpi)\exp(-i\varpi\tau + i\beta_2\varpi^2 z/2)\exp[ik_0(x-x')^2/2z]\mathrm{d}x'\,\mathrm{d}\varpi, \tag{1}$$

where $\tau = t - z/\tilde{v}$ stands for the local time in a frame moving at group velocity $\tilde{v}$; $\beta_2$ is a group velocity dispersion coefficient and $\varpi = \omega - \omega_0$ is a frequency relative to the carrier frequency. Further, $\Psi_0(x',\varpi)$ denotes the envelope at the source in the space-frequency domain. The second-order statistical properties of the ensemble $\{\Psi(x,\tau,z)\}$ at a given $z = \text{const}$ are described by the mutual coherence function, defined as $\Gamma(\mathbf{r}_1,\mathbf{r}_2) = \langle\Psi(x_1,\tau_1)\cdot\Psi^*(x_2,\tau_2)\rangle$, where $\mathbf{r}_1 = (x_1,\tau_1)$ and $\mathbf{r}_2 = (x_2,\tau_2)$ are two arbitrary space-time points in the $z$ plane and the angle brackets represent an ensemble average. Mathematically, the relative frequency $\varpi$ is a dummy integration variable in Eq. (1). In physics terms, though, distinct spectral components of a chirped source pulse arrive at a given transverse plane at different times and are therefore not temporally synchronized. It is then possible to introduce a linear frequency-to-time mapping, $\varpi = \kappa\tau'$ that defines an equivalent space-time source $\Psi_0(x',\varpi) \sim F(x',\tau')$. The proportionality constant $\kappa$ can be linked to a linear chirp of a Gaussian pulse through the relation $\kappa = 2\alpha/t_0^2$, where $\alpha$ is a pre-chirp parameter and $t_0$ is a temporal width of the unchirped pulse.[55] Accordingly, we can represent the mutual coherence function in the transverse plane $z = \text{const}$ by the expression

$$\Gamma(\mathbf{r}_1,\mathbf{r}_2,z) = \iint \Gamma_0(\mathbf{v}_1,\mathbf{v}_2)H(\mathbf{v}_1,\mathbf{r}_1)H^*(\mathbf{v}_2,\mathbf{r}_2)\mathrm{d}^2\mathbf{v}_1\,\mathrm{d}^2\mathbf{v}_2, \tag{2}$$

where $\mathbf{v} = (x',\tau')$, $\mathbf{r} = (x,\tau)$, and a spatiotemporal propagation kernel $H(\mathbf{r},\mathbf{v})$ has the form

$$H(\mathbf{r},\mathbf{v}) = (k_0\kappa^2/2\pi i z)^{1/2}\exp(ik_0x^2/2z)\exp(ik_0x'^2/2z + i\beta_2\kappa^2\tau'^2 z/2 - ik_0xx'/z - i\kappa\tau'\tau). \tag{3}$$

$\Gamma_0(\mathbf{v}_1,\mathbf{v}_2) = \langle F(\mathbf{v}_1)\cdot F^*(\mathbf{v}_2)\rangle$, where $F(\mathbf{v}) = \Psi_0(x',\kappa\tau')$, is an autocorrelation function of the envelope at two space-time points in the source plane. We refer to Eqs. (2) and (3) as a spatiotemporal van Cittert-Zernike theorem. The latter describes the evolution of spatiotemporal coherence properties of the ensemble on propagation in free space or a linear medium.[54,56] We can then define a complex degree of coherence (DOC) at a given pair of space-time points $(\mathbf{r}_1,\mathbf{r}_2,z)$ as[1,56]

$$\gamma(\mathbf{r}_1,\mathbf{r}_2) = \frac{\Gamma(\mathbf{r}_1,\mathbf{r}_2)}{\sqrt{I(\mathbf{r}_1)I(\mathbf{r}_2)}}, \tag{4}$$

where $I(\mathbf{r}) = \Gamma(\mathbf{r},\mathbf{r})$ is a field intensity of the wave packet. To generate a space-time partially coherent pulsed beam, we begin with a statistically stationary source that is incoherent in both space and time. The source is characterized by the correlation function $\Gamma_{\text{int}}(\mathbf{v}_1,\mathbf{v}_2)$ and can be modeled as an ensemble of scalar, randomly fluctuating realizations $\{F_n(\mathbf{v})\}_N$, such that $F_n(\mathbf{v}) = \sqrt{P(x',\kappa\tau')}e^{i\Theta_n(x',\kappa\tau')}$. $P(x',\kappa\tau')$ is a spectral density of the incoherent source, representing the power spectral density (PSD) function of the generated partially coherent space-time wave packet, which satisfies a standard nonnegativity requirement.[1] Random phases $\{\Theta_n(x',\kappa\tau')\}$ obey a zero-mean, unit-variance complex Gaussian probability distribution. On substituting from Eqs. (2) and (3) into Eq. (4) and performing algebraic calculations in a linear optical system, we obtain the complex DOC in the space-time domain as

$$\gamma(\mathbf{r}_1, \mathbf{r}_2) = \exp(ik_0 x_+ x_-/2z) \iint P(x', \kappa\tau') \exp[-i(k_0 x' \cdot x_-/z + \kappa\tau' \cdot \tau_-)] \mathrm{d}x' \, \mathrm{d}\tau', \tag{5}$$

where $x_\pm = x_1 \pm x_2$ and $\tau_- = \tau_1 - \tau_2$. The magnitude of the complex DOC, $|\gamma(\mathbf{r}_1, \mathbf{r}_2)| = |\gamma(x_-, \tau_-)|$. It follows at once from Eq. (5) that the PSD $P$ governs the distribution of the complex DOC, and the exponential terms determine the curvature of the wavefront and field correlations of the generated partially coherent wave packet. Given the ultrashort time scale of the pulsed field, implementing modulation in the frequency domain becomes a natural and efficient approach. In particular, the frequency-to-time mapping $\varpi(\tau') = \kappa\tau' = 2\alpha\tau'/t_0^2$ enabled by chirped pulses allows us to imprint complex spatiotemporal modulations directly to the pulsed fields by exploiting their time-dependent instantaneous frequency (Sec. 4).

To implement the space-time van Cittert-Zerike theorem and generate a space-time wave packet with a customized spatiotemporal coherence structure, we proceed by shaping a polychromatic pulsed beam. This is achieved using a holographic pulse shaper that incorporates a light modulator between a pair of diffraction gratings and cylindrical lenses in a $4f$ configuration depicted in Fig. 1. Under a strong linear chirp, the time-dependent instantaneous frequency of a fully coherent pulse is spatially dispersed by the first diffraction grating and cylindrical lens. As a result, the spectral dependence is mapped onto a "free" transverse spatial coordinate $\varpi(y')$ and different frequency components arrive at the SLM plane at distinct times, such that $\varpi(y') = 2\alpha\tau'/t_0^2$. In other words, modulation in the two-dimensional spatial domain $(x' - y')$ within the $4f$ pulse shaper is equivalent to modulation in the spatiotemporal domain $(x' - t')$. The corresponding instantaneous space-time field $F_n(\mathbf{v})$ is then synthesized by a hologram implementing a complex-amplitude modulation, given by $\sqrt{P[x', \varpi(y')]} e^{i\Theta_n[x', \varpi(y')]}$. This modulation produces a stochastic source with Gaussian statistics in the joint space-frequency (or equivalently, space-time) domain, owing to the one-to-one correspondence between the temporal frequency and time imposed by the linear chirp of the input pulse (Sec. 4). The resulting stochastic pulsed beam can be treated as a spatiotemporally incoherent source when the spectral and spatial widths of the wave packet on the hologram are larger than the corresponding characteristic scales of the random phases $\Theta_n[x', \varpi(y')]$ (see Note 2 in the Supplementary Material). This condition is satisfied in our experiment. After free space propagation through the second cylindrical lens and grating, the set of diffracted pulsed beams yields an ensemble of spatiotemporal wave packets with fluctuating intensity distributions and statistically stationary correlations in both space and time.

### 2.2 Experimental Realization

Any partially coherent light field can be constructed as an uncorrelated superposition of a set of coherent modes $\{\Psi_n(x, \tau, z)\}$.[1,57] Consequently, the essential step to generate a partially coherent wave packet with a tailored spatiotemporal coherence structure is a synthesis of these coherent modes. In Fig. 2, we show an experimental arrangement for generating partially coherent wave packets with a customized coherence structure. A pulsed beam with a ~20 nm bandwidth centered at 1030 nm, emitted from a mode-locked fiber laser, is split into two coherent replicas, an object pulse (red) and a probe pulse (blue), using a polarizing beam splitter (PBS). We exhibit time-integrated spatial intensity and power spectrum distributions of the pulse in Fig. 2(a). The object pulse is directed into a two-dimensional pulse shaper

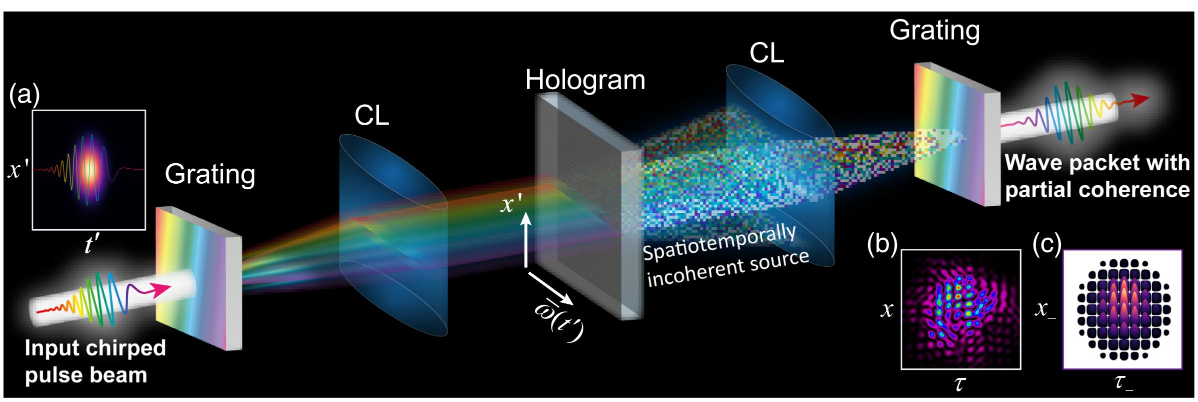


**Fig. 1** Schematic of the setup for implementing the spatiotemporal van Cittert-Zernike theorem to synthesize partially coherent space-time wave packets. A coherent chirped pulse beam (a) is first Fourier-transformed into its temporal frequency spectrum using a diffraction grating and a cylindrical lens (CL). The resulting space–spectral electric field is then modulated by a programmable complex hologram to impose a tailored coherence structure, producing a spatiotemporal incoherent pulsed source. Recombination of the spectrum through a second cylindrical lens and grating, followed by free-space propagation, reconstructs the pulse, yielding a wave packet with a tailored spatiotemporal coherence structure at the output plane of the axial-zero-order, characterized by a randomly fluctuating intensity distribution (b) and stationary statistical correlation (c) in both space and time.

displayed in Fig. 1, where we employ a phase-only spatial light modulator (SLM, Holoeye GAEA-2, $3840 \times 2160$ pixels with a 3.74 μm pitch and 60 fps) to tailor the space-frequency amplitude and wavefront of the input pulse according to the desired PSD function, implemented via the complex-amplitude holograms (Sec. 4). In Fig. 2(b), we show the time-integrated spatial and spectral intensity distributions after applying only the $\sqrt{P[x', \overline{\omega}(y')]}$ amplitude modulation, yielding a desired Gaussian profile as an example. As we apply a random phase modulation $\Theta_n[x', \overline{\omega}(y')]$, we generate, immediately past the SLM, an ensemble realization of the incoherent pulsed source with the instantaneous electric field exhibiting randomly fluctuating spatial and spectral intensities, as shown in Fig. 2(c). In practice, the power spectrum of $\Theta_n[x', \overline{\omega}(y')]$ is governed by a Gaussian distribution with a relatively narrow bandwidth (see Note 2 in the Supplementary Material for details). We generate a complete ensemble $\{\Psi_n(x, \tau)\}$ by sequentially refreshing the random phases $\Theta_n[x', \overline{\omega}(y')]$ on the hologram. At each step, we can view any individual realization $\Psi_n(x, \tau)$ as a coherent mode with a spatiotemporal profile fully retrievable using a Mach-Zehnder-like scanning interferometer. Briefly, the probe pulse passes through a pulse compressor composed of a parallel grating and a right-angle prism, which dechirps it into a Fourier-transform-limited pulse of ∼120 fs (much shorter than the duration of the objective wave packet). This probe pulse then interferes with the object pulse at a specific local time to produce interference fringes. By scanning the delay line, we can computationally reconstruct the spatiotemporal profile of each ensemble realization from the time-delay dependent interference patterns.

### 2.3 Spatiotemporal Manipulation of Coherence Width

To demonstrate the versatility of the proposed protocol for spatiotemporal DOC sculpting, we realize a partially coherent wave packet described by a generic Gaussian correlation function with tunable spatial and temporal coherence widths, yielding a spatiotemporal Gaussian Schell-model (STGSM) source. The DOC function of the STGSM wave packet is independent of a selected reference point and takes a concise Gaussian form as

$$\gamma(x_-, \tau_-) = \exp(-x_-^2/\delta_x^2 - \tau_-^2/\delta_\tau^2), \tag{6}$$

where $\delta_\tau$ and $\delta_x$ stand for temporal and spatial coherence widths. In Figs. 3(a) and 3(b), we show three-dimensional iso-intensity surface and phase distributions of an instantaneous ensemble realization of the generated STGSM ensemble. By combining the measured amplitude and phase, we obtain a joint probability

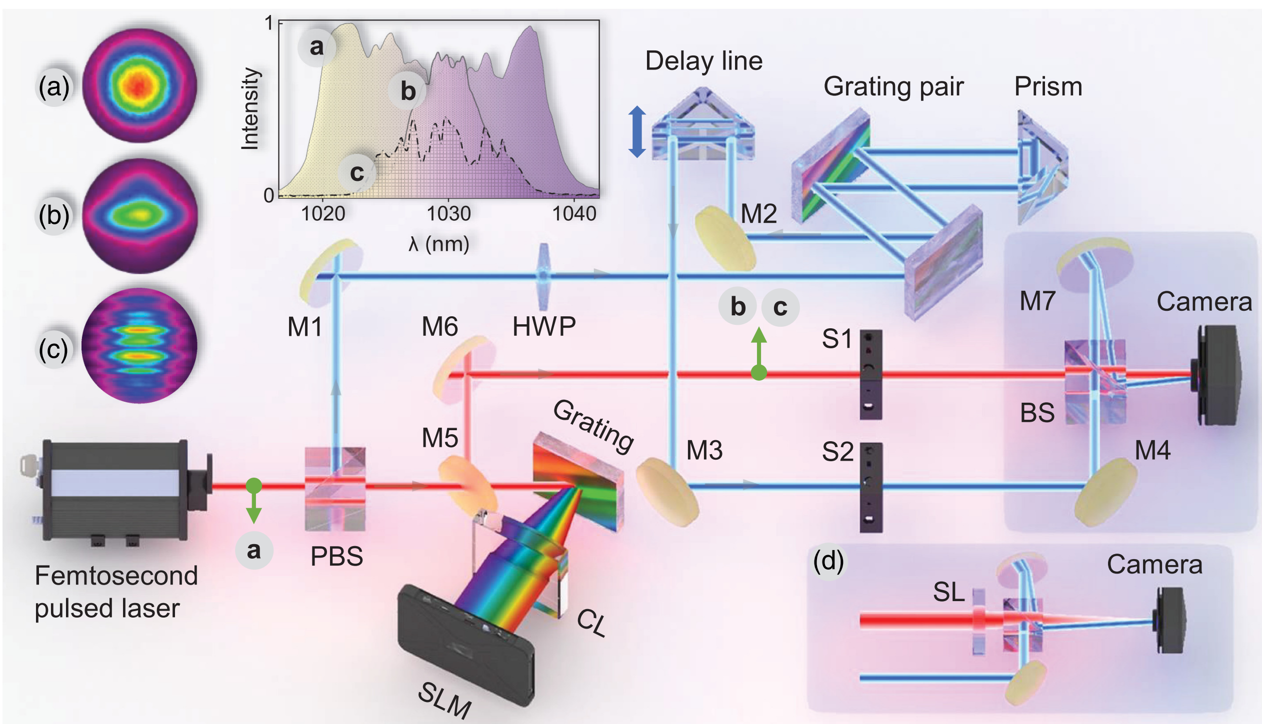


**Fig. 2** Experimental synthesis and characterization of partially coherent space-time wave packets with analysis of their propagation dynamics. The ensemble realization of the partially coherent wave packet is synthesized using a pulse shaper and characterized via a Mach-Zehnder-like scanning interferometer with a probe pulse. Its propagation dynamics are explored through free-space propagation and dispersion management. (a), (b), and (c) Spatial and spectral intensity distributions at specific locations. (d) Schematic of far field propagation of the generated partially coherent space-time wave packet. M1 – M7, planar mirror; S1, S2, shutters; PBS, polarizing beam splitter; BS, beam splitter; HWP, half-wave plate; CL, cylindrical lens with a focal length of 10 cm; SL, spherical lens with a focal length of 50 cm; SLM, spatial light modulator.

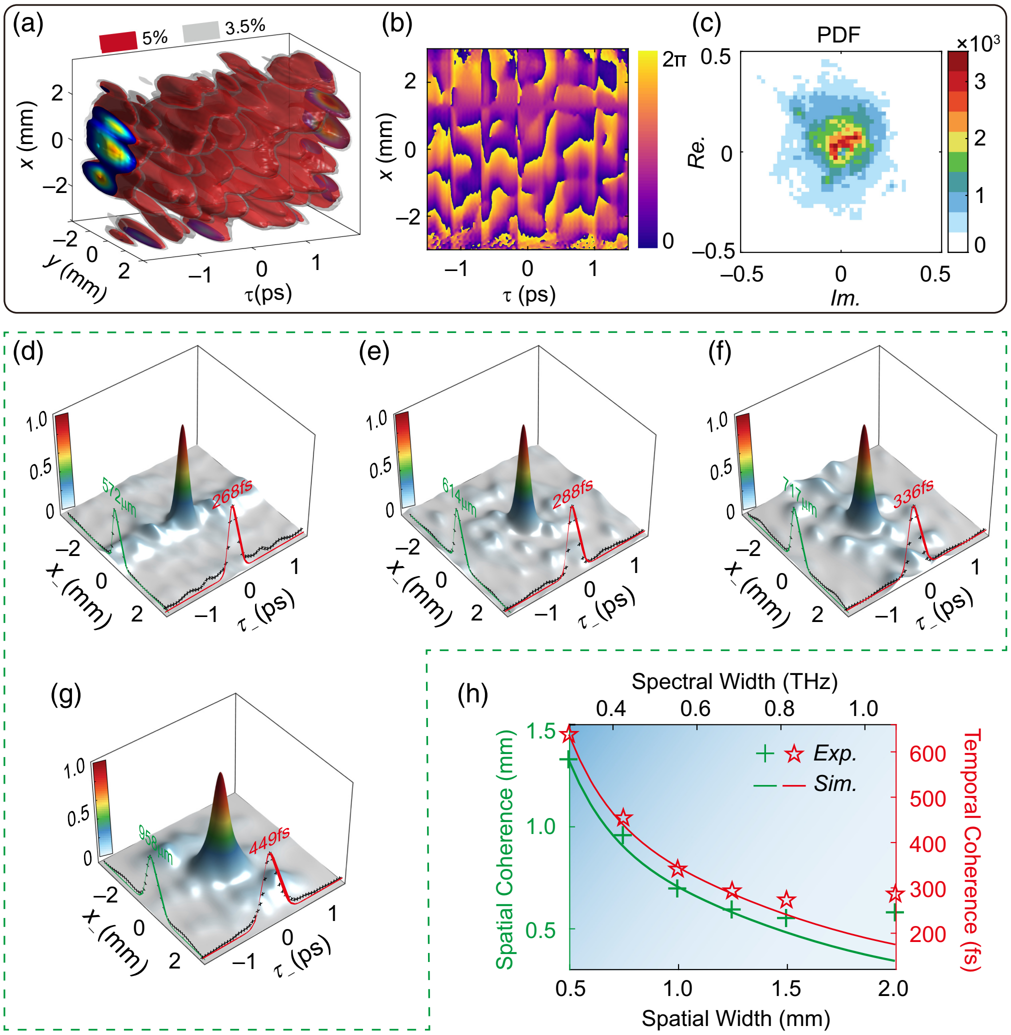


**Fig. 3** Manipulation of the spatiotemporal coherence width of an STGSM wave packet. (a) and (b) Intensity and phase (at $y = 0$) of an instantaneous ensemble realization of the generated STGSM wave packet. (c) The complex joint PDF calculated from (a) and (b) exhibits a circular Gaussian distribution, indicating that the speckle pattern follows Rayleigh statistics. Panels (d)–(g) show measured $|\gamma(x_-, \tau_-)|^2$ for different spatial and spectral widths of the PSD function [(d), (1.5 mm, 0.802 THz); (e), (1.25 mm, 0.684 THz); (f), (1 mm, 0.535 THz); (g), (0.75 mm, 0.401 THz)], with cross-lines and corresponding full widths at half maximum along space and time (the solid lines represent fitted curves corresponding to the dotted raw data). (h) Coherence width in both space $\delta_x$ and time $\delta_\tau$ as functions of the spatial and spectral widths of the PSD function. The solid lines represent the simulation results.

density profile (PDF), which is illustrated in Fig. 3(c). The PDF exhibits a circular Gaussian shape, confirming that the generated random wave packet by this method follows the Rayleigh statistics and corresponds to a statistically stationary, homogeneous field.[5,57] Consequently, $|\gamma(x_-, \tau_-)|^2$ can be inferred from the normalized second-order intensity correlation function, which, in turn, can be evaluated from the intensity autocorrelation $I_n(x, \tau) \otimes I_n(x, \tau)$ of the ensemble of the stationary, homogeneous fields (see Note 3 in the Supplementary Material for details). Figures 3(d)–3(g) present our experimental results for $|\gamma(x_-, \tau_-)|^2$ for variable spatial and spectral widths of the PSD function, where the dotted and solid curves denote the cross-lines of the raw data and a Gaussian fit. The measured $|\gamma(x_-, \tau_-)|^2$ exhibits a bell (Gaussian) shape in both space and time as the generated partially coherent wave packet is accurately described by the Gaussian Schell-model. The full width at half maximum of the Gaussian fit quantifies the DOC in both space and time. As the spatial and spectral widths of the PSD function increase, the spatiotemporal widths of DOC fall off. In Fig. 3(h), we compare the simulated and experimental results for the spatiotemporal coherence width for variable spatial and spectral widths of the PSD function. A close agreement between the experiment and simulations demonstrates that the spatiotemporal coherence widths can be monotonically tuned by adjusting the PSD function of the partially coherent wave packet. We note that the minimum achievable coherence widths in space and time are constrained by the finite spatial-spectral extent of the input pulsed beam.

### 2.4 Spatiotemporal Manipulation of Coherence Structure

Beyond the demonstrated ability to tune the coherence widths in both space and time, our framework can be readily adapted to tailor the spatiotemporal coherence structure of any partially coherent wave packet. To showcase this capability, we generate a space-time Hermite-Gaussian correlated Schell-model ($\mathrm{STHGCSM}_{m,n}$) wave packet as a representative example, whose target spatiotemporal DOC function is defined as

$$\gamma(x_-,\tau_-) = \frac{H_{2m}(x_-/\sqrt{2}\delta_x)H_{2n}(\tau_-/\sqrt{2}\delta_\tau)}{H_{2m}(0)H_{2n}(0)}\exp\left(-\frac{x_-^2}{2\delta_x^2}-\frac{\tau_-^2}{2\delta_\tau^2}\right), \tag{7}$$

where $H_m(\cdot)$ denotes a Hermite polynomial of order $m$; $\delta_\tau$ and $\delta_x$ are temporal and spatial coherence widths, respectively. In the limiting case of $m = n = 0$, the $\mathrm{STHGCSM}_{0,0}$ reduces to a generic STGSM wave packet [Eq. (6)]. In Fig. 4(a), we display the instantaneous intensity of a single ensemble realization of the generated $\mathrm{STHGCSM}_{1,1}$ wave packet. The experimental and simulated results for $|\gamma(x_-,\tau_-)|^2$ of $\mathrm{STHGCSM}_{1,1}$ wave packet follow in Figs. 4(b) and 4(c), respectively. In addition, we also produce HG-correlated partially coherent wave packets of variable orders $m$ and $n$, with the corresponding $|\gamma(x_-,\tau_-)|^2$ distributions shown in Figs. 4(d)–4(f). We observe excellent agreement between the experimentally generated and simulated spatiotemporal coherence structures, which all feature non-Gaussian envelopes,

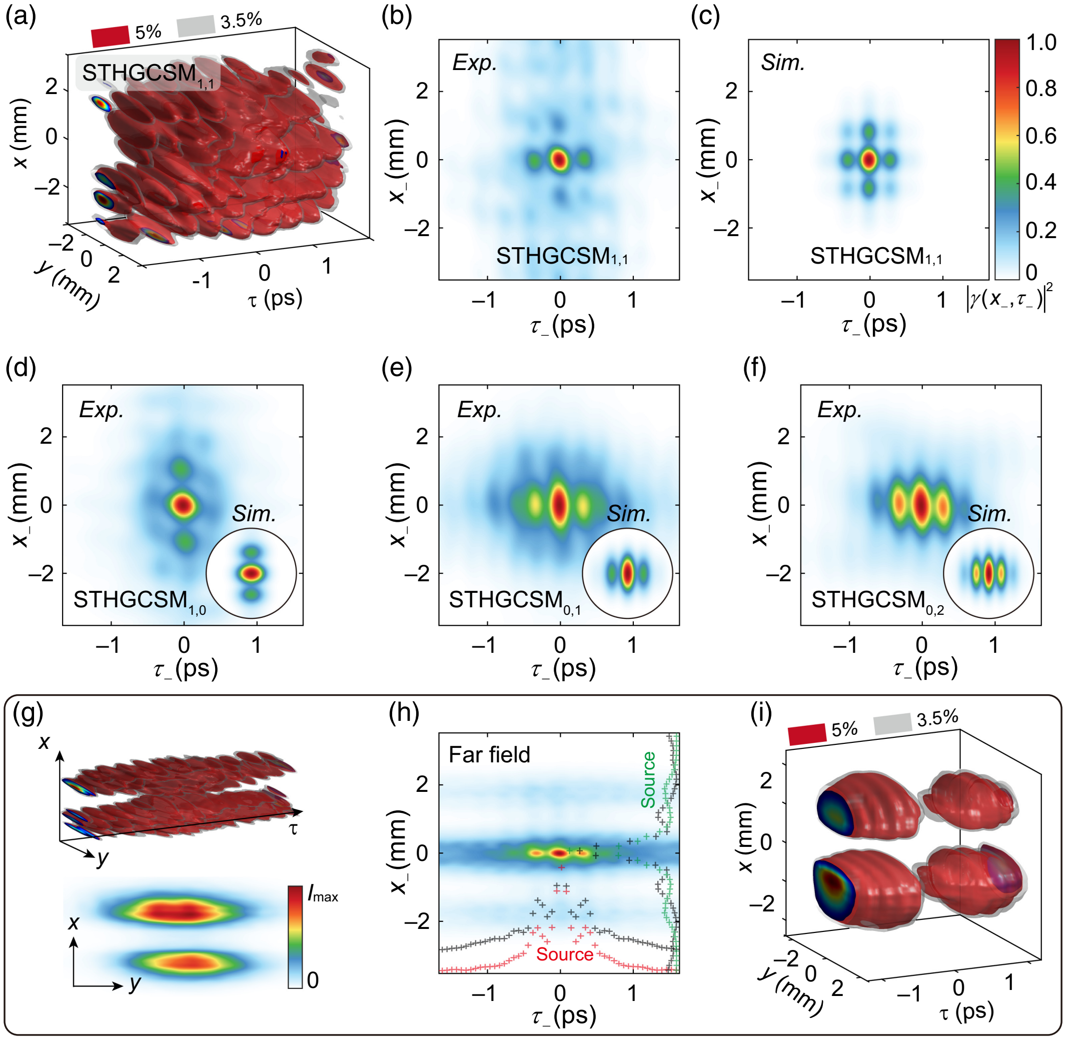


**Fig. 4** Manipulation of the spatiotemporal coherence structure of an $\mathrm{STHGCSM}_{m,n}$ wave packet and its propagation dynamics analysis. (a) Intensity of an instantaneous ensemble realization of the generated $\mathrm{STHGCSM}_{m,n}$ wave packet. (b) Measured and (c) simulated $|\gamma(x_-,\tau_-)|^2$ of the $\mathrm{STHGCSM}_{m,n}$ wave packet. (d)–(f) Measured and simulated $|\gamma(x_-,\tau_-)|^2$ for $\mathrm{STHGCSM}_{m,n}$ with different orders. (g) Instantaneous intensity and corresponding time-integrated intensity of an $\mathrm{STHGCSM}_{1,1}$ wave packet after free-space propagation to the far field. (h) Measured distribution of coherence structure after free-space propagation to the far field, where the dark (colorful) dotted lines denote cross-sections of $|\gamma(x_-,\tau_-)|^2$ after free propagation (at the source). (i) Three-dimensional iso-intensity surface (ensemble averaged over 50 realizations) of the generated $\mathrm{STHGCSM}_{1,1}$ wave packet after propagation under anomalous dispersion.

confirming a successful generation of HG-correlated structures in both space and time.

Instructively, the spatiotemporal coherence structure governs the evolution of the intensity profile of a partially coherent wave packet in space and time. To illustrate this point, we experimentally study the propagation characteristics of the generated STHGCSM wave packets in dispersionless and anomalously dispersive regimes. We show a schematic of the free-space propagation setup in Fig. 2(d). A spherical lens is employed to examine the far-field evolution. On the other hand, temporal dispersion of the medium can be engineered in free space by encoding a pre-chirp phase term $\exp(i\beta_2\varpi^2 z/2)$ onto the hologram.[39] First, when the $\mathrm{STHGCSM}_{1,1}$ wave packet propagates to the focal plane of the lens in free space (without dispersion), the resulting far-field instantaneous three-dimensional iso-intensity surface (top) and the time-integrated intensity distribution directly recorded by the camera (bottom) are shown in Fig. 4(g). Due to the absence of temporal dispersion, the partially coherent wave packet with the HG-correlated structure splits into only two distinct spatial lobes while preserving its temporal profile. In this case, unlike conventional two-dimensional transverse spatial evolution, the duality between the spatial and temporal diffusion equations is completely broken,[58] resulting in asymmetric propagation dynamics in the spatial and temporal domains. Consequently, the coherence structure $|\gamma(x_-, \tau_-)|^2$ in the far-field remains unchanged in the temporal dimension, but is significantly degraded spatially due to diffraction, as demonstrated in Fig. 4(h). Notably, preserving the temporal coherence structure enables confidential data transport in free space. To this end, the statistical DoFs of light serve as controllable information channels.[16,17] In the anomalously dispersive regime in the presence of a group delay dispersion of 0.5 $\mathrm{ps}^2$, the $\mathrm{STHGCSM}_{1,1}$ wave packet splits into two distinct lobes in both space and time, yielding a characteristic four-lobe intensity profile (consistent with the simulation results provided in Note 4 in the Supplementary Material). This behavior is experimentally confirmed in Fig. 4(i), which shows measurements obtained by ensemble averaging over 50 realizations.

## 3 Discussion and Conclusion

In conclusion, we have advanced theoretically and demonstrated experimentally a protocol to modulate the spatiotemporal coherence of random light fields within the framework of the spatiotemporal analogue of the classic van Cittert-Zernike theorem that we have formulated. By imprinting a random wavefront with designed amplitude modulation onto an input chirped laser pulse, we have attained precise control over the spatiotemporal coherence width and structure of the resulting statistically stationary, homogeneous wave packet. We have experimentally demonstrated the generation of space-time Gaussian Schell-model sources with tunable spatial and temporal coherence widths, as well as the wave packets featuring Hermite-Gaussian field correlations of variable order in both spatial and temporal dimensions. The propagation dynamic of these partially coherent wave packets qualitatively differs from that of quasimonochromatic partially coherent beams with the same structure of spatial field correlations. Specifically, during free-space propagation, the coherence structure degrades spatially due to diffraction but remains intact temporally. In the anomalous dispersion regime, the spatiotemporal coherence structure, in turn, actively governs the evolution of the light field in both space and time.

Notably, the partially coherent space-time wave packets demonstrated here are spatiotemporally separable in both their intensity and correlation structures. However, this framework can be readily extended to spatiotemporally nonseparable states by adopting a coupled PSD function. Besides, the generated partially coherent space-time wave packets exhibit a nearly uniform intensity distribution across the spatiotemporal plane. Overcoming this limitation will be crucial for fully unlocking the potential of these intriguing forms of structured light. In addition, although the square of the modulus of the coherence structures is characterized through autocorrelation operations, the DOC is inherently a complex-valued quantity. A complete characterization of its real and imaginary components generally requires extensive statistical averaging over many realizations, making the measurement process time-consuming. This limitation may be alleviated by implementing self-reference-based measurement schemes.[5,21]

Our work can be distinguished from the first experimental demonstration of spatiotemporal coherence manipulation in a broadband incoherent field generated by a statistically stationary LED source by Yessenov et al.[48] In Ref. 48, partial spatial coherence is tightly linked to temporal incoherence through ingenious spatiotemporal spectral correlations. In this paper, we have employed a narrowband and chirped ultrafast pulsed source to produce statistically stationary wave packets of light of controllable spatiotemporal coherence with the aid of judicious frequency-to-time mapping. Furthermore, our protocol enables access to both spatial and temporal coherence, rendering the tailored coherence structure spectrally independent. This capability may facilitate precise synchronization of interacting partially coherent pulses and enhance the efficiency of nonlinear processes.[51,52] Moreover, the proposed scheme for spatiotemporal coherence manipulation can be extended to other incoherent sources,[50] such as random lasers, LEDs, and ASE sources, to sculpt sophisticated partially coherent space-time light fields or tailor the speckle statistics. In addition, the synthesis speed and efficiency can be further boosted by integrating a 2D holographic pulse shaper with high-speed modulators, nanophotonic platforms, and multimode optical systems.[59] Such advancements may unlock promising applications in coherent quantum control, light-matter interactions, and nonlinear imaging in multiple-scattering media, and provide deeper insights into fundamental phenomena such as light transport properties.[51,60,61]

## 4 Appendix: Methods

### 4.1 Spatiotemporal Synthesis Using a Spatial Light Modulator

In the experiment, we used a chirped Gaussian pulse beam from a lab-built fiber laser source, with a spatial rms radius of ∼2 mm and a spectral bandwidth of ∼20 nm centered at 1030 nm [Fig. 1(a)]. The pulse, having a linear pre-chirp of $+0.045\ \mathrm{ps}^2$ (while higher-order dispersion terms can be neglected in dilute air) and a Fourier-transform-limited duration of 120 fs, is incident at an angle of $\theta_i = 46$ deg onto a reflective blazed grating with a groove density of $N = 1200$ lines/mm. This pre-chirp can be precisely controlled through group-delay-dispersion engineering using an SLM. The first-order diffraction ($m = +1$) disperses the beam horizontally, providing a spectral angular resolution of $\Delta\theta_d/\Delta\lambda = mN/\cos\theta_i = 0.08$ deg/nm. The dispersed beam is subsequently collimated by a cylindrical lens with a focal length of $f = 100$ mm and projected onto an SLM with a pixel pitch of 3.74 μm, covering a spatial extent of $\Delta L = 2f \tan \Delta\theta_d/2 = 2.8$ mm. This setup yields a frequency-to-pixel mapping of $\omega_p = 4.76 \times 10^{-5}$ rad fs$^{-1}$ pixel$^{-1}$ on the SLM. The angular frequency corresponding to the central wavelength is identified by introducing a $0 - \pi$ phase step at $y = y_0$. Consequently, the applied frequency coordinate is related to the physical spatial coordinate through $\varpi(y') = \omega_p(y' - y_0')/3.74$, which gives rise to the space-to-time mapping: $\tau_y' = t_0^2 \varpi(y')/2\alpha$. This relation establishes a direct correspondence between spatial modulation at the pulse shaper and the effective temporal coordinate of the chirped pulse. The chirp (dispersion) coefficient is incorporated into the calculation of the corresponding complex amplitude function as a scaling parameter, thereby eliminating the influence of the initial pulse chirp on the generation of coherent structures.

### 4.2 Precise Spatial-Spectral Control for Generating an Incoherent Source $\Gamma_{int}(\mathbf{v}_1, \mathbf{v}_2)$

To generate an incoherent source characterized by $\Gamma_{\text{int}}(\mathbf{v}_1, \mathbf{v}_2)$, we express the field of the source as a superposition of uncorrelated coherent modes, such that $\Gamma_{\text{int}}(\mathbf{v}_1, \mathbf{v}_2) = \langle F_n(\mathbf{v}_1) \cdot F_n^*(\mathbf{v}_2) \rangle$, where $F_n(\mathbf{v})$ represents a random realization of the incoherent source,[59] expressed as $F_n(\mathbf{v}) = \sqrt{P(x', \kappa\tau')} e^{i\Theta_n(x', \kappa\tau')}$. The set of random phases $\{\Theta_n\}$ is assumed to obey a Dirac delta correlation, ensuring statistical independence of different realizations. To synthesize the field $F_n(\mathbf{v})$ of the incoherent source in the $(x', \tau')$ plane, we exploit the linear temporal dependence of the instantaneous frequency inherent to a linearly chirped ultrafast pulse. Owing to this property, the space-time modulation of $F_n(\mathbf{v})$ can be equivalently implemented as a purely spatial modulation through the space-to-time (frequency) mapping, yielding $F_n(\mathbf{v}) = \sqrt{P[x', \varpi(y')]} e^{i\Theta_n[x', \varpi(y')]}$. To encode the spatial-spectral wavefront of the input pulsed beam into the above coherent modes, a set of phase-only holograms $\exp(i\Phi_n)$ is produced using the following complex-amplitude algorithm, given by[31,58,62]

$$\Phi_n(x', y') = \operatorname{mod}\left\{ \Theta_n[x', \varpi(y')] + \pi \cdot \operatorname{sinc}^{-1}\sqrt{P[x', \varpi(y')]} - g_0 x' \operatorname{sinc}^{-1}\sqrt{P[x', \varpi(y')]}, 2\pi \right\}, \tag{8}$$

where $\operatorname{sinc}^{-1}(\cdot)$ is an inverse sinc function (see Note 5 in the Supplementary Material) and $g_0$, the frequency of a linear phase ramp, the depth of which is contingent upon the PSD function. $\varpi(y') = \kappa\tau' = 2\alpha\tau'/t_0^2$ represents the mapping from a physical spatial coordinate to a temporal frequency (see Sec. 4.1). In the SLM, $\Theta_n$ can be approximated as a colored-noise phase with a narrow bandwidth (see Note 2 in the Supplementary Material).

## Disclosures

The authors declare no competing interests.

## Code and Data Availability

The data that support the findings of this study are available from the authors upon reasonable request.

## Authors' Contributions

X.L. and Y.C. initiated the project and developed the theory. X.L. conducted the simulations and experiments. X.L., W.L., C.L., and Y.Z. completed the data analysis and visualizations. X.L., S.A.P., Q.Z., and Y.C. contributed to drafting and finalizing the manuscript. S.A.P., Q.Z., and Y.C. supervised the project. All authors participated in the discussion and review of the manuscript.

## Acknowledgments

This work was supported by the National Natural Science Foundation of China (Grant Nos. W2441005 [Y.C.], 12534014 [Y.C.], 12434012 [Q.Z.], 62535013 [Q.Z.], 12192254 [Y.C.], and 12547149 [X.L.]), the National Key Research and Development Program of China (Grant No. 2022YFA1404800 [Y.C.]), the Natural Science Foundation of Shandong Province (Grant Nos. ZR2025ZD21 [Y.C.] and ZR2023YQ006 [C.L.]), and the Key Research and Development Program of Shandong Province (Grant No. 2024JMRH0105 [Y.C.]). S.A.P. acknowledges support from the Natural Sciences and Engineering Research Council of Canada (RGPIN-2025-04064). X. Liu acknowledges Dr. Haihao Fan at the University of Shanghai for Science and Technology for his assistance with the visualization of Fig. 2.

## References

1. E. Wolf, *Introduction to the Theory of Coherence and Polarization of Light*, Cambridge University Press (2007).
2. A. Forbes, M. D. Oliveira, and M. R. Dennis, "Structured light," *Nat. Photonics* **15**, 253–262 (2021).
3. C. He, Y. Shen, and A. Forbes, "Towards higher-dimensional structured light," *Light Sci. Appl.* **11**, 205 (2022).
4. J. Wang, K. Li, and Z. Quan, "Integrated structured light manipulation," *Photonics Insights* **3**, R05 (2024).
5. X. Liu et al., "Measurement of optical coherence structures of random optical fields using generalized Arago spot experiment," *Opto. Electro. Sci.* **2**, 220024 (2023).
6. M. Araki et al., "Optical coherence tomography in coronary atherosclerosis assessment and intervention," *Nat. Rev. Cardiol.* **19**, 684–703 (2022).
7. J. N. Clark et al., "High-resolution three-dimensional partially coherent diffraction imaging," *Nat. Commun.* **3**, 993 (2012).
8. M. Pascucci et al., "Compressive three-dimensional super-resolution microscopy with speckle-saturated fluorescence excitation," *Nat. Commun.* **10**, 1327 (2019).
9. J. Bertolotti et al., "Non-invasive imaging through opaque scattering layers," *Nature* **491**, 232–234 (2012).
10. O. Katz et al., "Non-invasive single-shot imaging through scattering layers and around corners via speckle correlations," *Nat. Photonics* **8**, 784–790 (2014).
11. Y. R. Lee et al., "Exploiting volumetric wave correlation for enhanced depth imaging in scattering medium," *Nat. Commun.* **14**, 1878 (2023).
12. Y. Cai and S. Y. Zhu, "Ghost imaging with incoherent and partially coherent light radiation," *Phys. Rev. E* **71**, 056607 (2005).
13. G. Ma et al., "Unidirectional imaging with partially coherent light," *Adv. Photonics Nexus* **3**, 066008 (2024).
14. Y. Peng et al., "Speckle-free holography with partially coherent light sources and camera-in-the-loop calibration," *Sci. Adv.* **7**, eabg5040 (2021).
15. Z. Shi et al., "Super-resolution orbital angular momentum holography," *Nat. Commun.* **14**, 1869 (2023).
16. D. Peng et al., "Optical coherence encryption with structured random light," *PhotoniX* **2**, 6 (2021).
17. X. Liu et al., "Unlocking secure optical multiplexing with spatially incoherent light," *Laser Photonics Rev.* **19**, 2401534 (2025).
18. S. Lin et al., "Statistically stationary random light for high-security encryption," *Optica* **12**, 1261–1268 (2025).

19. X. Lu et al., "Coherence entropy during propagation through complex media," *Adv. Photonics* **6**, 046002 (2024).
20. M. Batarseh et al., "Passive sensing around the corner using spatial coherence," *Nat. Commun.* **9**, 3629 (2018).
21. X. Lu et al., "Noniterative spatially partially coherent diffractive imaging using pinhole array mask," *Adv. Photonics* **1**, 016005 (2019).
22. R. C. Charles, S. Fan, and D. Miller, "Measuring, processing, and generating partially coherent light with self-configuring optics," *Light Sci. Appl.* **13**, 260 (2024).
23. X. Zhao et al., "Ultrahigh precision angular velocity measurement using frequency shift of partially coherent beams," *Laser Photonics Rev.* **17**, 2300318 (2023).
24. B. Dong et al., "Partial coherence enhances parallelized photonic computing," *Nature* **632**, 55–62 (2024).
25. X. Liu et al., "Axial correlation revivals and number factorization with structured random waves," *Phys. Rev. Appl.* **20**, L021004 (2023).
26. M. S. S. Rahman et al., "Universal linear intensity transformations using spatially incoherent diffractive processors," *Light Sci. Appl.* **12**, 195 (2023).
27. X. Liu, Q. Cao, and Q. Zhan, "Spatiotemporal optical wavepackets: from concepts to applications," *Photonics Insights* **3**, R08 (2024).
28. Q. Zhan, "Spatiotemporal sculpturing of light: a tutorial," *Adv. Opt. Photonics* **16**, 163–228 (2024).
29. A. Forbes, "Structured light in space and time," *Photonics Insights* **4**, C02 (2025).
30. A. Chong et al., "Generation of spatiotemporal optical vortices with controllable transverse orbital angular momentum," *Nat. Photonics* **14**, 350–354 (2020).
31. X. Liu et al., "Spatiotemporal optical vortices with controllable radial and azimuthal quantum numbers," *Nat. Commun.* **15**, 5435 (2024).
32. W. Chen et al., "Time diffraction-free transverse orbital angular momentum beams," *Nat. Commun.* **13**, 4021 (2022).
33. H. E. Kondakci and A. F. Abouraddy, "Diffraction-free space–time light sheets," *Nat. Photonics* **11**, 733–740 (2017).
34. M. Yessenov et al., "Space-time wave packets," *Adv. Opt. Photonics* **14**, 455–570 (2022).
35. M. Yessenov et al., "Veiled talbot effect," *Phys. Rev. Lett.* **125**, 243901 (2020).
36. L. A. Hall et al., "The space-time talbot effect," *APL Photonics* **6**, 056105 (2021).
37. C. Wan et al., "Toroidal vortices of light," *Nat. Photonics* **16**, 519–522 (2022).
38. W. Chen et al., "Observation of chiral symmetry breaking in toroidal vortices of light," *Phys. Rev. Lett.* **132**, 153801 (2024).
39. X. Liu et al., "Dynamics of photonic toroidal vortices mediated by orbital angular momenta," *Sci. Adv.* **11**, eadz0843 (2025).
40. X. Liu et al., "Ultrafast bursts of tailored spatiotemporal vortex pulses," *Light Sci. Appl.* **14**, 361 (2025).
41. F. Feng et al., "Spatiotemporal optical vortex combs," *Nat. Commun.* **16**, 11652 (2025).
42. Y. Shen, H. Wang, and S. Fan, "Free-space topological optical textures: tutorial," *Adv. Opt. Photonics* **17**, 295–374 (2025).
43. H. Teng et al., "Construction of optical spatiotemporal skyrmions," *Light Sci. Appl.* **14**, 324 (2025).
44. M. Yessenov et al., "Ultrafast space-time optical merons in momentum-energy space," *Nat. Commun.* **16**, 8592 (2025).
45. Y. Zhou et al., "Spatiotemporally localized optical links and knots," *Nat. Commun.* (2026).
46. G. Gui et al., "Second-harmonic generation and the conservation of spatiotemporal orbital angular momentum of light," *Nat. Photonics* **15**, 608–613 (2021).
47. R. Martín-Hernández et al., "Extreme-ultraviolet spatiotemporal vortices via high harmonic generation," *Nat. Photonics* **19**, 817–824 (2025).
48. M. Yessenov et al., "Non-diffracting broadband incoherent space–time fields," *Optica* **6**, 598–607 (2019).
49. H. Wang et al., "Coloured vortex beams with incoherent white light illumination," *Nat. Nanotechnol.* **18**, 264–272 (2023).
50. C. W. Chen et al., "Output control of dissipative nonlinear multimode amplifiers using spacetime symmetry mapping," *Nat. Phys.* **21**, 839–845 (2025).
51. M. Mounaix et al., "Spatiotemporal coherent control of light through a multiple scattering medium with the multispectral transmission matrix," *Phys. Rev. Lett.* **116**, 253901 (2016).
52. Z. Pang and A. Arie, "Coherence synthesis in nonlinear optics," *Light Sci. Appl.* **14**, 101 (2025).
53. V. Aita, "Nobel 2005: coherence and precision spectroscopy," *Nat. Rev. Phys.* **7**, 534 (2025).
54. C. You et al., "Multiphoton quantum van Cittert-Zernike theorem," *npj Quantum Inf.* **9**, 50 (2023).
55. A. M. Weiner, *Ultrafast Optics*, Wiley (2011).
56. M. Born and E. Wolf, *Principles of Optics: Electromagnetic Theory of Propagation, Interference and Diffraction of Light*, Elsevier (2013).
57. F. Wang et al., "Three modal decompositions of Gaussian Schell-model sources: comparative analysis," *Opt. Express* **29**, 29676–29689 (2021).
58. W. Chen et al., "Tailoring spatiotemporal wavepackets via two-dimensional space-time duality," *Nat. Commun.* **16**, 2818 (2025).
59. L. Liu et al., "Ultra-robust informational metasurfaces based on spatial coherence structures engineering," *Light Sci. Appl.* **13**, 131 (2024).
60. Y. Fang, Z. Lyu, and Y. Liu, "Ultrafast physics with structured light," *Nat. Rev. Phys.* **7**, 713–727 (2025).
61. X. Xie and Y. Shen, "Topological light waves manipulating particles: a perspective," *Light Manip. Appl.* **1**, 202501 (2026).
62. Q. Cao et al., "Spatiotemporal hologram," *Nat. Commun.* **15**, 7821 (2024).
63. P. De Santis et al., "An example of a Collett-Wolf source," *Opt. Commun.* **29**, 256–260 (1979).
64. F. Wang et al., "Experimental generation of partially coherent beams with different complex degrees of coherence," *Opt. Lett.* **38**, 1814–1816 (2013).
65. G. W. Goodman, *Statistical Optics.* Wiley (2015).
66. A. Papoulis, *Probability, Random Variables, and Stochastic Processes*, McGraw Hill (1991).
67. F. Wang and O. Korotkova, "Convolution approach for beam propagation in random media," *Opt. Lett.* **41**, 1546–1549 (2016).
68. J. A. Davis et al., "Encoding amplitude information onto phase-only filters," *Appl. Opt.* **38**, 5004–5013 (1999).



**Xin Liu** is currently a lecturer in the School of Physics and Optoelectronics at Shandong Normal University. He received his PhD in optics from Shandong Normal University in 2025. His research interests focus on the manipulation and applications of structured light fields, including statistical optics, partially coherent light, spatiotemporal structured light fields, and ultrafast optics.

**Sergey A. Ponomarenko** is a professor in the Department of Electrical and Computer Engineering and Department of Physics and Atmospheric Science, Dalhousie University, Canada. He had served as a Canada Research Chair from 2006 to 2016. He heads Theoretical Optics and Photonics Group (TOP) at Dalhousie. His research interests include structured light, optical coherence theory, phase-space description of classical and quantum light, classical and quantum entanglement, and wave packet revivals.

**Qiwen Zhan** is chair professor of nanophotonics in the Department of Electronic and Information Engineering at the Westlake University. He serves as the PI and the founding director of the Complex Optical Fields and Meta-Optical Structures (COSMOS) laboratory. His research

interests include spatially and spatiotemporally structured light, ultrafast optics, and nanophotonics.

**Yangjian Cai** is a professor of optics in the School of Physics and Optoelectronics at Shandong Normal University, where he also serves as vice president of the university. He is the founding director of the Shandong Provincial Engineering and Technology Center for Light Manipulation. His research interests include light manipulation and applications, optical coherence and polarization, atmospheric optics, laser physics, and optical imaging.

Biographies of the other authors are not available.